3D surface reconstruction of liquid structures in sprays using structured illumination and phase demodulation

Adrian Roth*[1], Edouard Berrocal[1]
[1]Lund University, Department of Physics, Division of Combustion Physics, Lund, Sweden
*Corresponding author: adrian.roth@forbrf.lth.se

Abstract
The accurate surface reconstruction of 3D liquid structures is an important aspect for the understanding of spray formation and liquid breakups. In this article, an approach to image in 3D the surface of liquid structures in sprays (such as ligaments, liquid sheets/cores and liquid blobs) is presented. The technique is named Fringe Projection - Laser Induced Fluorescence (FP-LIF) which is used by illuminating the liquid structures using a laser interference fringe projection. By doping, at high concentration, the injected liquid with a fluorescent dye (here fluorescein) a fluorescence signal can be generated very close to the liquid surface. Then, this signal is recorded at a backward angle where the incident modulation encodes the information of the third surface coordinate for each pixel. The recorded 2D images are phase demodulated using the Continuous Wavelet Transform (CWT) and the 3D surface coordinates can be retrieved. In the first part of the presented work, simulated liquid surfaces are considered for parameter optimization of the 3D reconstruction and to evaluate the CWT implementation. It is found from the simulated results that the optimum fringe projection period sampling is $4-7$ pixels. In the second part, the technique is applied for two experimental cases of a pending drop and for an onion shaped liquid sheet. To conclude, both the simulated and experimental results show promising 3D reconstructions of liquid surfaces providing a new type of data, which in the future can be used for the validation of computational models simulating liquid breakup.

Keywords
3D reconstruction; liquid structures; phase demodulation; Continuous Wavelet Transform; Fringe Projection; Laser Induced Fluorescence.

Introduction

Understanding the formation of a spray system as well as characterizing its overall structure requires the use of advanced imaging techniques. Over the past three decades, a variety of approaches have been employed to obtain either two-dimensional (2D) or three-dimensional (3D) spray characteristics. Examples of 2D imaging techniques are: transillumination (line of sight) imaging, such as white light shadowgraphy or Ballistic imaging and planar imaging techniques (optical sectioning), such as laser sheet Mie Scattering and Planar Laser Induced Fluorescence (PLIF) as reviewed by Linne [1] and Fansler et al. [2]. Though, as sprays have complex inhomogeneous structures in 3D space, 2D imaging is not sufficient if one desire to obtain a complete and faithful visualization of the liquid bodies present in such systems and 3D imaging is in this case highly desirable. The spray region is located further down from the nozzle orifice and is composed of a cloud of already formed microscopic droplets. This structure can be reconstructed in 3D by extracting the extinction coefficient as explained by Grosshans et al. in [3]. The experimental data of the extinction coefficient can be used in the validation of numerical models, where the models simulate the process of liquid atomization and droplet transport. Since the extinction coefficient is dependent on both the spray droplet number density and droplet size the experimental results will not directly validate a model but it will indicate if a model is incorrect. One approach to experimentally measure the local extinction coefficient in 3D is to stack a number of planar images using Structured Illumination Planar Imaging (SLIPI) allowing suppression of light intensity from multiple scattering as demonstrated by Wellander et al. [4]. The slicing starts with an optical sectioning at the edge of the spray, where the attenuation of the light from the laser sheet to the camera is assumed to be negligible. The remaining slices use the estimated local extinction coefficients of all previous slices to correct for light attenuation in the spray volume between the slice and the camera. A different approach for 3D estimation of the local extinction coefficient in 3D is through backwards projection from transmission imaging, using the Computed Tomography (CT) technique as demonstrated by Marchitto et al. in [5] and Kristensson et al. in [6]. In this case the spray injection nozzle is rotated for each tomographic view and images are averaged over several injection events. To be able to obtain single-shot 3D images of transient events, the CT technique can be used with multiple cameras instead of rotating the nozzle as shown by by Halls et al. in [7] where a tracer concentration in a turbulent gaseous free jet is reconstructed in 3D. With instantaneous imaging this method can reconstruct each unique jet with a temporal resolution of 50 μs, which is achieved using several

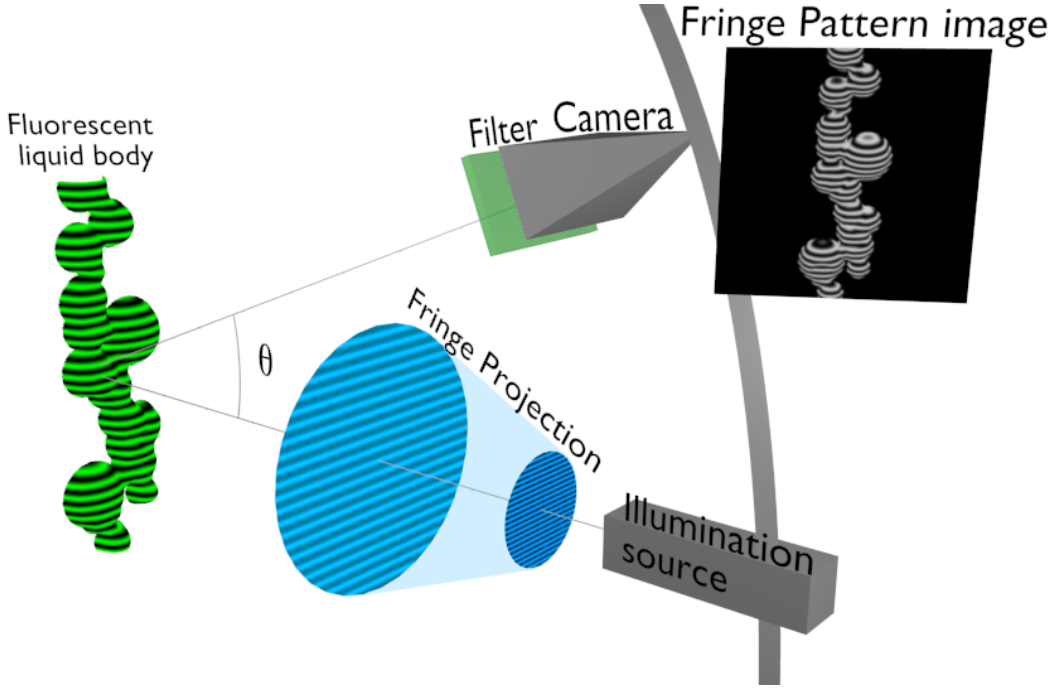

Figure 1. Illustration of the setup for the 3D reconstruction FP-LIF technique. The fringe projection illuminates a 3D structure, here simulated random spheres further explained in the simulation results, and fluorescence is only induced close to the surface as a result of high concentration of the fluorescent component. The projected fringes are imaged from an angle θ through a filter which only transmits the fluorescing wavelength. The resulting captured image can be modelled by Eq. (1) where the phase ϕ is proportional to the third coordinate of the structure if a telecentric setup is used to record the image. The phase is extracted by using an image phase demodulation method.

(in this case 8) high speed cameras. Even with this approach there are limitations in the 3D spatial resolution which depends on the number of views as concluded by Mohri et al. in [8] for a similar CT algorithm. As a means of avoiding the limitations of the mentioned 3D reconstructions techniques and provide an additional validation tool for numerical spray models, the goal of this article is to present the development of the Fringe Projection - Laser Induced Fluorescence (FP-LIF) technique which can reconstruct the surface of 3D (liquid) structures with visible light from just one image, one camera and give a resulting 3D coordinate for each image pixel.

Description of the FP-LIF technique

Each pixel in an image has two coordinates where generally the third world coordinate is missing. The third surface coordinate of a structure can be encoded into an image using the fringe projection structured illumination as illustrated in the FP-LIF setup in Figure 1. The LIF is an approach to deal with issues connected to imaging light reflected from surfaces, especially when transparency and specular reflection are involved. With a high concentration of fluorescence dye on the object surface the projected fringes are only absorbed and emitted close to the surface and with a filter in front of the camera the reflected light is removed and only the back fluorescence is imaged.

The captured image with this technique shown in Figure 1 can be modelled by a fringe pattern as seen in Eq. (1). The first part in the cosine expression is the carrier which is set along the y direction with horizontal lines to match the camera position on top of the fringe projector. If the camera is on the side of the projector vertical lines is preferred since horizontal ones will not encode the correct information. Then, for the foreground, A is the background illumination, B is the modulation amplitude, T is the carrier period and the background is simply modelled noise ϵ. For the 3D reconstruction technique the phase ϕ is the essential part since it, for the telecentric case, is proportional to the object's third coordinate as shown by Takeda et al. in [11] and with a calibration real 3D coordinates can be calculated for each image pixel. The method for extracting the phase in the image I is called phase demodulation.

$$I(x,y) = \begin{cases} A(x,y) + B(x,y)\cos\left(\dfrac{2\pi}{T}y + \phi(x,y)\right) + \epsilon(x,y), & (x,y) \in \text{foreground} \\ \epsilon(x,y), & (x,y) \in \text{background} \end{cases} \tag{1}$$

Phase Demodulation

The technique of extracting 3D coordinates by phase demodulation of a fringe projection illumination is not new. Multiple phase demodulation methods have been developed in the past and they all have the same goal: To extract the phase ϕ from an image of a fringe pattern, in this case a carrier fringe pattern, which is the one showed as foreground in Eq. (1).

a) Review of methods

A first class of methods for phase demodulation are phase-stepping methods where multiple images are used to extract the phase, one example is given by Zhang et al. in [9]. Each image has a different phase shift of the fringes and at least three images are required to find a unique solution for A, B and ϕ for every pixel. One advantage with this approach is that the phase can be extracted independently pixel by pixel. However the limitation, in the case of spray application, is that multiple images need to be recorded for each demodulation and 3D reconstruction. As previously mentioned the need of multiple images for one 3D reconstruction is not desired for the case of instantaneous imaging of fast moving liquid flows. Instead a single image phase demodulation method is required.

One class of single image demodulation methods is called Regularized Phase Trackers. The approach iteratively finds the phase for each pixel from minimizing an energy function [12]. This method has best performance compared to other phase demodulation methods when used on the so-called closed fringe patterns where the fringes has no certain direction. For Eq. (1) this means that the carrier is removed by setting the period T to infinity. Limitations of the method are the requirement of parameter initialisation and in some cases pre-normalisation of the fringe pattern [12]. Since this work use images with carrier fringes, the Regularized Phase Tracker methods are not used.

The phase demodulation method used in this article is the Continuous Wavelet Transform (CWT) method. This method is connected to the Fourier methods first introduced by Takeda et al. [11], mostly known as the Fourier Transform (FT) method. The FT method take the Fourier transform of the image and after filtering and inverse Fourier transform the parameters of the fringe pattern, A, B and ϕ, can be estimated. The method is computationally fast but its greatest weakness is connected to the spatial localisation of the demodulation [12][13][14]. Put in other words, the filtering in the frequency domain has no control of where in the spatial domain these frequencies exists and errors might leak into spatial structures. One way to solve this is by using the Windowed Fourier Transform (WFT) methods which tries to gain localisation in the spatial domain where the FT method has none, as demonstrated by Qian in [14] and by Zhong et al. in [12]. The WFT approach is very similar to the CWT approach where the CWT also has the option of using waves with no certain direction, isotropic wavelets, which is why the CWT method is used in this work. The next section will cover a more detailed explanation of the Continuous Wavelet Transform phase demodulation method.

b) The Continuous Wavelet Transform method

The implementation of the CWT method depends on the theory of wavelets where a wavelet is a general word for a wave-like oscillation package. One example is the 2D Mexican Hat wavelet, a real valued function found in Eq. (2) and illustrated in Figure 2. It is isotropic which means that it is rotational invariant.

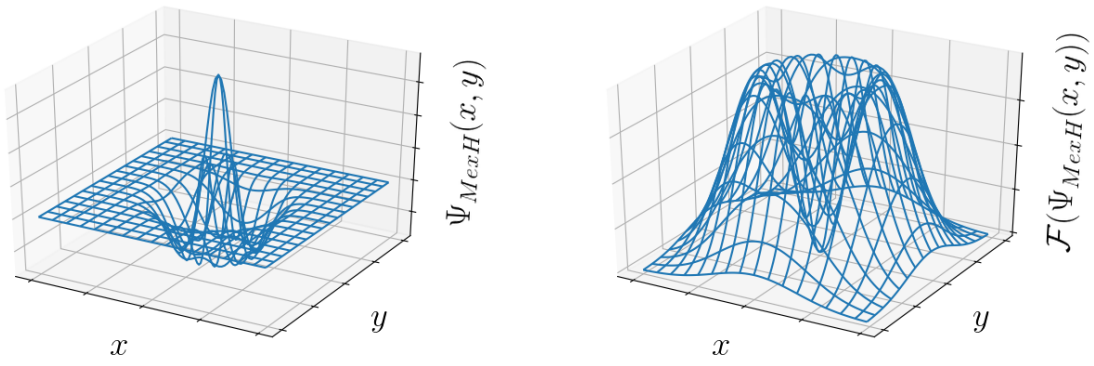

Figure 2. Visual examples of the Mexican Hat wavelet, the function on the left and the Fourier transform of the wavelet on the right.

$$\Psi_{MexH}(x,y) = (1-(x^2+y^2))\exp\left(-\frac{1}{2}\left(x^2+y^2\right)\right). \tag{2}$$

The wavelet contains properties such as maximum absolute amplitude at the origin and a mean value equal to zero. Each wavelet can be scaled and/or translated which gives birth to children of the original mother wavelet and the children are created as,

$$\Psi_{a,\boldsymbol{b}}(\boldsymbol{x}) = \frac{1}{a}\Psi\left(\frac{\boldsymbol{x}-\boldsymbol{b}}{a}\right), \tag{3}$$

where a is the scaling parameter, $\boldsymbol{b}$ is the translation parameter and Ψ is the mother wavelet function. In general a is a real positive non zero value and $\mathbf{b}$ can also be any real value but it is usually connected to a discrete sampled signal, such as an image, and will take integer values of the sample or pixel coordinate.
With wavelets the Continuous Wavelet Transform (CWT) of a function f is calculated as

$$W_f(a,\mathbf{b}) = \int\int f(\mathbf{x})\frac{1}{a}\Psi^*\left(\frac{\mathbf{x}-\mathbf{b}}{a}\right)d^2\mathbf{x}. \tag{4}$$

From a 2D signal the transform is a function with three dimensions, one for the scale a and two for the translation $\mathbf{b}$. In addition one can rotate the wavelet as a fourth dimension, but this is not necessary for our isotropic wavelet. Here each $W_f(a,\mathbf{b})$ for each combination of a and $\mathbf{b}$ is named the wavelet coefficient and together all coefficients absolute values are known as the scalogram.
With the theory of wavelets and the Continuous Wavelet Transform one approach to demodulate the phase $\phi(\mathbf{x})$ in an image is firstly to find the ridge of the scalogram which is calculated as

$$R(\mathbf{b}) = \text{argmax}_a(|W_f(a,\mathbf{b})|). \tag{5}$$

In other words the Ridge is the wavelet with scale a which best match the fringe pattern frequency at pixel $\mathbf{b}$. This is the heaviest computational step and with the use of an isotropic wavelet one dimension is dropped which limits the search space. From the ridge the wrapped phase is estimated with the phase method as described by Watkins in [12] as

$$\hat{\phi}'_{wrapped}(\mathbf{x}) = \arg(W_f(R(\mathbf{x}),\mathbf{x})). \tag{6}$$

Two important things to note is that firstly ϕ' includes both information of the phase ϕ and the carrier, $\frac{2\pi}{T}y$ in Eq. (1) and secondly that the signal is wrapped in the interval $(-\pi,\pi]$ as a result of taking the argument of a complex number. The wrapped phase is unwrapped using a scikit-image algorithm [15] and finally the carrier, which is assumed to be known through image pre-processing, is subtracted.
The wavelet used in this report is a semi-isotropic version of the Mexican hat wavelet which is complex valued, compared to the real valued one in Eq. (2); and its Fourier transform is given in Figure 3. It is calculated by taking the Mexican Hat wavelet and in the frequency domain remove all coefficients with negative x frequency. Since this wavelet is no longer isotropic rotation will make a difference. However since the method demodulates a carrier fringe pattern, where at maximum half of the frequency directions are used, it is sufficient to know the general direction of the fringe pattern and rotate all wavelet scales to this direction.

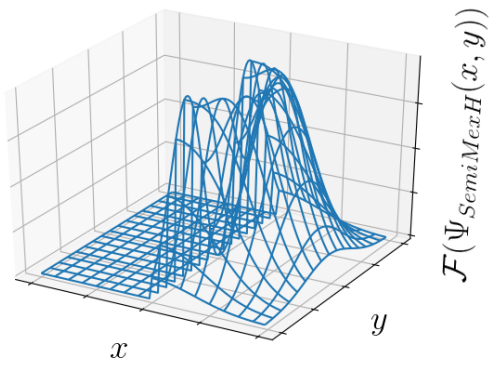

Figure 3. Fourier transform of the semi Mexican Hat wavelet used for its complex property in the spatial domain together with its 180^o angle distribution.

At last it is considered how the CWT is most efficiently implemented. A fast implementation is to use the Fast Fourier Transform (FFT) and the convolution theorem of the Fourier transform as concluded by Watkins in [12]. The continuous wavelet transform can be calculated as a 2D convolution as seen in Eq. (4) and with the Fourier convolution theorem the result is

$$W_f(a) = a\mathcal{F}^{-1}(\mathcal{F}(f)\mathcal{F}(\Psi^*)) \tag{7}$$

for all pixels and single scale a. This is the implementation used for the phase demodulation results provided in the next sections.

Simulated Results

The first demodulations are of 3D structures corresponding to random spheres. As the name suggests the real simulated 3D structure is a sum of random spheres, an example is shown in Figure 4 where the 3D structure is on the left and a scaled version of it is used as the phase ϕ for the fringe pattern in the middle with carrier period $T = 5$ pixels. The resulting phase demodulation using the CWT method is shown as the rightmost image in the same Figure. The demodulation is successful down to an error of 2% (0.3 radians) in general for the whole structure and up to 10% (1.5 radians) close to the edges. Note that the input image has no noise at all. The larger errors close to the edges are probably a combination of invalid black pixels used in the demodulation together with a large phase derivative which is a challenge for the demodulation method.
A second challenge for the demodulation method is to choose the carrier period T. The quality of the phase demodulation is largely dependent on this parameter which means that it should be tuned for optimal reconstruction. In this article the optimal period T is found using the simulated random spheres 3D structure seen in Figure 4 and fringe patterns with different carrier periods where in addition different noise levels are simulated for each T. The noise levels are calculated using the Signal to Noise Ratio: $SNR = \dfrac{B^2}{2\sigma_\epsilon^2}$, and σ_ϵ^2 is the variance of normal distributed noise ϵ seen in Eq. (1). For each combination of SNR and T a 3D reconstruction is performed and the RMS error to the correct structure is calculated for all valid pixels. The result is shown in Figure 5. The optimal fringe period length seems to be between 4-7 pixels. In general the reconstruction gets worse with more noise but it is interesting to see that both for too high and low carrier period length, compared to the optimal interval, are more sensitive to noise. Note that these results are only valid for the simulated random spheres 3D structure shown in Figure 4, however similar results are given by different simulations of random spheres. For a real spray structure the optimal carrier length might be different, but this optimal carrier period is used as guidance for the experimental setup.

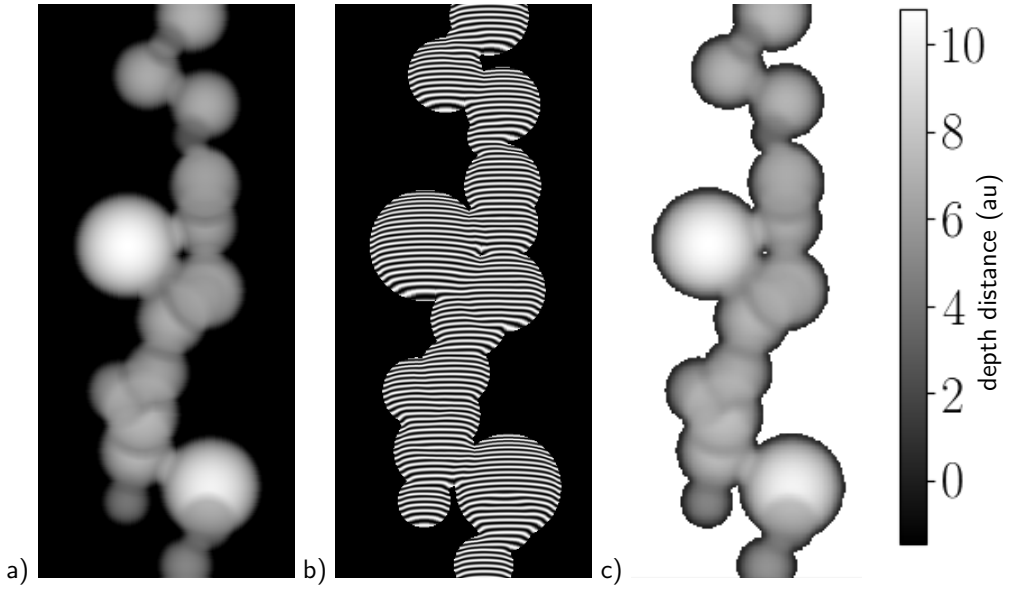

Figure 4. One example of the random spheres simulated 3D structure (a) where the white pixels are closest to the camera and black furthest away. The random spheres method is a simple simulation of falling liquid with random spatially located spheres added together as the 3D structure. For this example all black pixels around the structure in the left image are classified as invalid background, they are not used in the error calculation for the 3D reconstruction. Now a scaled version of the 3D structure is also used as the phase ϕ in Eq. 1 to simulate a fringe projection (b) with the carrier period $T = 5$ pixels. The phase demodulation of the fringe pattern is shown in (c) where the white areas are invalid background pixels. The demodulation manages to reconstruct the structure of the original phase but it has a larger difficulty with the pixels close to the invalid areas.

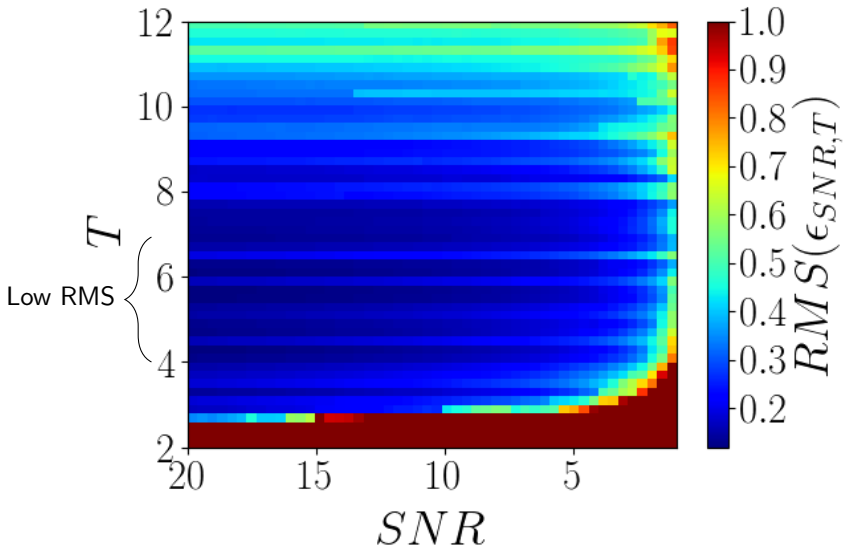

Figure 5. The root mean square errors of the phase demodulation of the 3D structure in Figure 4 with different combinations of SNR and fringe pattern period length T. The error is thresholded to a maximum of 1 for improved colour resolution of the best combinations. In general lower SNR results in larger error and in addition it seems that too low and too high fringe pattern periods are more sensitive to noise. The optimal fringe pattern period length seems to be between 4-7 pixels for this input random spheres 3D structure.

Experimental Results

The experimental setup used is similar to the illustration shown in Figure 1 though the camera is on the side rather than on top of the illumination direction, this is the reason for not using horizontal lines which would not encode the correct information in the image. Instead diagonal lines are used and they work for either of the two camera locations. The first experimental result is shown in Figure 6 where the 3D reconstruction of pending drop is seen and the fringe pattern period length is around 20 pixels. Secondly a recorded image of an onion shaped spray, with the width of around 25 mm, is shown as the leftmost image in Figure 7 where the period length of the fringe pattern is around 6 pixels. Both Figures include the original recorded image where the brighter parts are ones manually segmented prior to the reconstruction. This means that the interesting areas of the image were noted and then used in the 3D reconstruction, similar to the methodology for the random spheres demodulation in the last section. Only parts of the images with clear fringe pattern are segmented as foreground. The other images in the Figures are visualisations of the resulting 3D reconstruction, here imaged with a virtual camera in the 3D computer graphics software Blender. For the result in Figure 7 the setup was calibrated so that the angle $\theta \approx 16^o$.

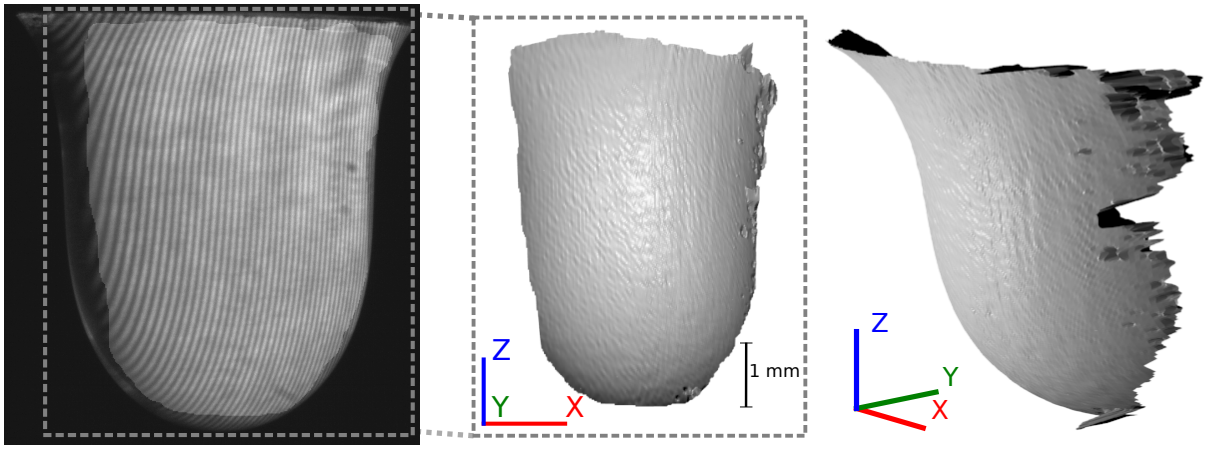

Figure 6. The top image show experimental data of a pending liquid drop imaged with the Fringe-Projection. The corresponding 3D reconstruction from the front side and slightly rotated are shown at the bottom. The brighter area in the top image is the segmented foreground of the image and the rest of the image does not show the pattern. The reconstruction has been virtually imaged in the 3D computer graphics software Blender.

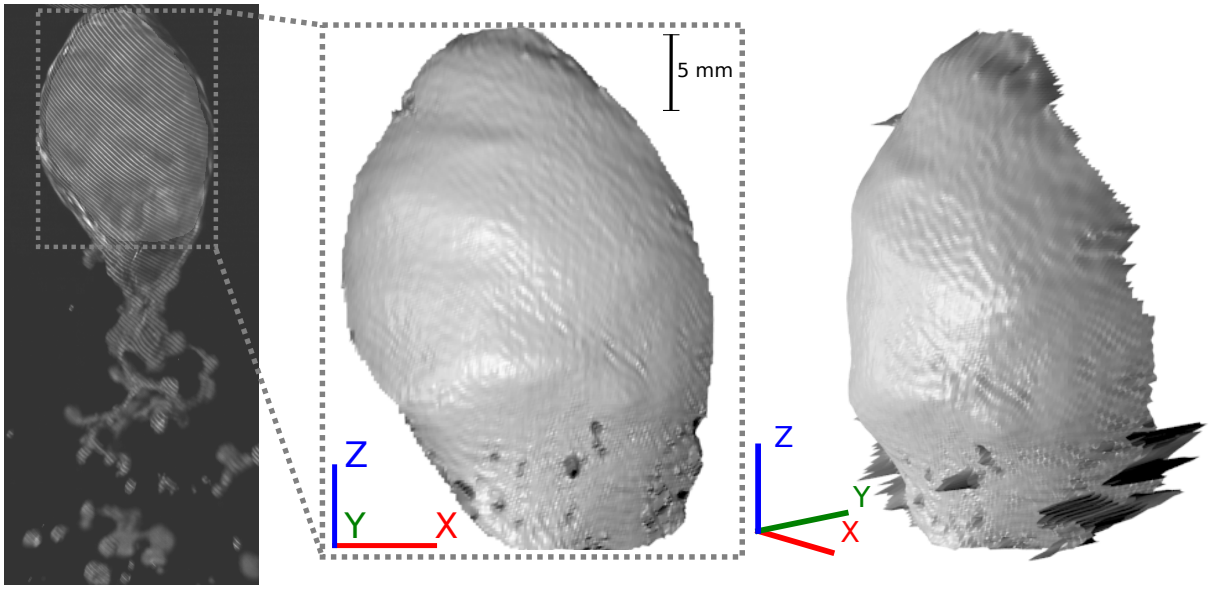

Figure 7. Experimental results of an onion shaped spray, similarly visualised as in Figure 6, with a width of around 25 mm. The leftmost image show the imaged fringe pattern and the right images shows its corresponding 3D reconstruction from the front side and slightly rotated. Even though this data is recorded with a perspective lens, telecentricity is assumed since the camera and projector source distance to the surface is much larger than the surface depth.

Conclusions

To advance the understanding of the spray systems and characterizing its structure the FP-LIF technique is presented for reconstructing the 3D surface coordinates of a spray. The technique use fringe projection on a structure with high concentration of fluorescent dye. The imaged fringe pattern has encoded information of the 3D structure as the phase of this pattern. This phase is estimated through a phase demodulation method called the Continuous Wavelet Transform method which is used with the semi-isotropic Mexican hat wavelet. The results on the simulated data shows that the technique reconstructs the 3D structures correctly. In addition it is concluded that the projected fringe pattern carrier period length is optimal between 4 and 7 pixels for the random spheres 3D structure. For the experimental results there are features, small bumps and larger spikes, which might be connected to errors in the demodulation. The future development of the technique will aim towards understanding why the results include these features and, if they are connected to errors in the reconstruction, how they can be removed. Generally the FP-LIF technique is promising for future application where high speed measurements of liquid breakups will be included for 4D experimental data.

Acknowledgements

This work was supported by grants from the Swedish Research Council - Vetenskapsrådet (VR Grant 2016-03894) and from the H2020 European Research Council (ERC-Starting Grant "Spray-imaging" number 638546). The authors would also like to thank Dr. Jan Jedelský and Marcel Sapík for their support in gathering experimental data of the onion shaped spray.

Nomenclature

θ	angle between fringe projection direction and camera direction
T	fringe pattern period [pixels]
x	the horizontal pixel direction in an image [pixels]
y	the vertical pixel direction in an image, positive direction is from top to bottom of image [pixels]
$A(x,y)$	background illumination of imaged fringe pattern [image intensity]
$B(x,y)$	fringe pattern modulation amplitude [image intensity]
$\phi(x,y)$	fringe pattern phase [radians]
$\epsilon(x,y)$	noise in the imaged fringe pattern with zero mean and Variance σ_ϵ^2, $SNR = \frac{B^2}{2\sigma_\epsilon^2}$ [image intensity]
$\Psi_{(MexH)}$	Wavelet function (for the Mexican Hat wavelet)
$\mathcal{F}(f)$	Fourier transform of function f
$\mathbf{x}$	(x,y) vector
a	scaling factor for the child wavelet

$\mathbf{b}$ translation vector (b_x, b_y) for the child wavelet
$W_f(a, \mathbf{b})$ wavelet coefficient of function f with child wavelet of scale a and translation $\mathbf{b}$
$R(\mathbf{b})$ ridge of scalogram in the CWT phase demodulation method

References

[1] Linne, M., 2013, "Imaging the Optically Dense Regions of a Spray: A Review of Developing Techniques," Progress in Energy and Combustion Science, 39(5), pp. 403-440.

[2] Fansler, T. D. and Parrish, S. E., 2015, "Spray Measurement Technology: a Review," Measurement Science and Technology, 26.

[3] Grosshans, H., Kristensson, E., Szász, R.-Z. and Berrocal, E., 2015, "International Journal of Multiphase Flow," 72, pp. 218-232,

[4] Wellander, R., Berrocal, E., Kristensson, E., Richter, M. and Aldén, M., 2011, "Three-dimensional measurement of the local extinction coefficient in a dense spray," Measurement Science and Technology, 22(12).

[5] Marchitto, L, Allocca, L, Hampai, D, Alfuso, S, Dabagov, SB, Liedl, A and Polese, C, 2015, "3D Structure of Liquid Sprays: X-ray μ-radiography and Tomography by Polycapillary based Technique," Nuclear Inst. and Methods in Physics Research, B, 355, pp. 285–288.

[6] Kristensson, E., Berrocal, E. and Aldén, M., 2012, "Quantitative 3D Imaging of Scattering Media using Structured Illumination and Computed Tomography," Optics Express, 20(13), pp. 14437–14450.

[7] Halls, B. R., Gord, J. R., Meyer, T. R., Thul, D. J., and Slipchenko, M. and Roy, S., 2017, "20-kHz-rate Three-Dimensional Tomographic Imaging of the Concentration Field in a Turbulent Jet," Proceedings of the Combustion Institute, 36, pp. 4611–4618.

[8] Mohri, K., Görs, S., Schöler, J., Rittler, A., Dreier, T., Schulz, C. and Kempf, A., 2017, "Instantaneous 3D Imaging of Highly Turbulent Flames using Computed Tomography of Chemiluminescence," Applied Optics, 56(26), pp. 7385–7395.

[9] Zhang, S. and Yau, S.-T., 2006 "High-resolution, real-time 3D absolute coordinate measurement based on a phase-shifting method," Opt. Express 14, pp. 2644-2649.

[10] Meadows, D. M., Johnson, W. O. and Allen, J. B., 1970, "Generation of Surface Contours by Moiré Patterns," Applied Optics, 9(4), pp. 942–947.

[11] Takeda, M. and Mutoh, K., 1983, "Fourier Transform Profilometry for the Automatic Measurement of 3-D Object Shapes," Applied Optics, 22(24), pp. 3977-3982.

[12] Pramod K. Rastogi and Erwin Hack, 2015, *Phase Estimation in Optical Interferometry*, Boca Raton : CRC Press, Chap. 2,3 and 5.

[13] Liu, F., Wu, Y., Wu, F., Wan, Y., Xu, Y., König, N. and Schmitt, R., 2018, "Precise phase demodulation of single carrier-frequency interferogram by pixel-level Lissajous figure and ellipse fitting," Scientific Reports, 8(1).

[14] Kemao, Q., 2007, "Two-dimensional windowed Fourier transform for fringe pattern analysis: Principles, applications and implementations," Optics and Lasers in Engineering, 45, pp. 304–317.

[15] van der Walt, S., Schönberger, J. L., Nunez-Iglesias, J., Boulogne, F., Warner, J. D., Yager, N., Gouillart, E., Yu T. and the scikit-image contributors, 2014, "scikit-image: Image processing in Python," PeerJ 2:e453.